Journal of Alloys and Compounds 688 (2016) 118–122

Contents lists available at ScienceDirect

Journal of Alloys and Compounds

journal homepage: http://www.elsevier.com/locate/jalcom

Magnetocrystalline anisotropy in $Gd(Co,Fe)_{12}B_6$: A first-principles study

X.B. Liu*, Z. Altounian, D.H. Ryan

Centre for the Physics of Materials and Department of Physics, McGill University, Montreal, Quebec, H3A 2T8, Canada

ARTICLE INFO

Article history:
Received 21 May 2016
Received in revised form
13 July 2016
Accepted 14 July 2016
Available online 17 July 2016

Keywords:
$GdCo_{12}B_6$
Magnetocrystalline anisotropy
Substitution energy
DFT+U
Rare earth

ABSTRACT

The electronic structure, preferential site occupancy for Fe, and magnetocrystalline anisotropy (MCA) have been investigated in $Gd(Co_{12-x}Fe)_xB_6$ *via* a DFT (density functional theory) plus Hubbard U approach (DFT + U). For Gd atoms, the spin-up 4*f* bands are fully occupied while the spin-down 4*f* hole levels are completely empty. The *d*-like states dominate at the Fermi Level, mainly contributed by Co(Fe) 3*d* electrons. Co atoms in $GdCo_{12}B_6$ carry magnetic moments of − 0.3 μ_B and − 0.7 μ_B at the 18*g* and 18*h* sites respectively, while the 7.3 μ_B Gd moments are ordered antiparallel to the Co(Fe) sublattice. The DFT total energy calculations show that the Fe atoms prefer to replace Co at the 18*h* site rather than the 18*g* site, with an energy gain of 0.16 eV/f.u. and they carry a magnetic moment of 1.5 μ_B/Fe. $GdCo_{12}B_6$ shows a weak easy *c*− axis MCA (E_{mca} = 90 μeV/f.u.) while $GdCo_{11}FeB_6$ displays a moderate easy *ab*− plane MCA (E_{mca} = −2690 μeV/f.u.). The spin reorientation induced by Fe doping is related to the electronic structure change near Fermi Level and the different contributions of Co and Fe to the MCA in $GdCo_{12-x}Fe_xB_6$.

1. Introduction

Since the discovery of the $Nd_2Fe_{14}B$ permanent magnet [1–3], significant research effort has been devoted to R-Co-B and R-Fe-B based magnetic systems. In addition to their important technological performance, their intrinsic magnetic properties such as exchange interactions, magnetic anisotropy and ordering behavior, have been intensively investigated. The ternary boride system, $RCo_{12}B_6$, was first identified by Niihara and Yajima [4] and later found to form with iron by Buschow et al. during a survey of the Nd-Fe-B ternary phase diagram [5]. $RTM_{12}B_6$ adopts the trigonal $SrNi_{12}B_6$ structure (space group $R\bar{3}m$ #166) with the transition metal (TM) occupying the 18*g* and 18*h* sites, the rare earth (R) occupying the 3*a* and the boron atom at the 18*h* site [6–13].

The $RCo_{12}B_6$ compounds exist for the entire rare earth series with lattice parameters that follow the conventional lanthanide contraction [7]. They are all collinear ferro- (La-Sm) or ferri- (Gd-Tm) magnets with rather small cobalt moments of 0.4 μ_B and modest ordering temperatures T_C of about 150 K [7]. Mössbauer measurements on ^{57}Fe-doped materials suggested that for R = Y, La, Sm, Gd, Tb, and Er, the ordering was in the basal plane [10,14,15]. However, compounds with R = Nd appeared to exhibit axial ordering at 4.2 K, but reoriented into the basal plane on heating [10]. Recently however, both ^{155}Gd Mössbauer spectroscopy [16] and neutron diffraction [17] showed that the magnetic ordering direction of $GdCo_{12}B_6$ was in fact axial (*i.e.* parallel to the *c*− axis) and that basal plane ordering only developed when the system was doped with iron. As little as 4% Fe (0.5 Fe/f.u.) was sufficient to drive the axial to basal plane transition [16,17]. As the ordering directions for the other $RCo_{12}B_6$ compounds have all been derived from ^{57}Fe-doped samples, a re-evaluation of these compounds may be necessary.

As part of our endeavor is to understand the magnetocrystalline anisotropy (MCA) in $RCo_{12}B_6$, we have investigated the MCA by a first-principles DFT calculation. In this paper, we report on the electronic structure, Fe preferential site occupancy, and the MCA effects of both the structural distortion and electronic changes induced by Fe doping in $GdCo_{12-x}Fe_xB_6$.

2. Methodology and computational details

The first-principles electronic structure calculations were performed in the framework of density functional theory (DFT). The QUANTUM ESPRESSO package [18], in the projector augmented wave (PAW) framework [19], was employed to perform DFT

* Corresponding author.
E-mail addresses: liux@physics.mcgill.ca (X.B. Liu), zaven.altounian@mcgill.ca (Z. Altounian), dominic@physics.mcgill.ca (D.H. Ryan).

http://dx.doi.org/10.1016/j.jallcom.2016.07.143
0925-8388/

calculations using the generalized gradient approximation (GGA) of Perdew-Burke-Ernzerhof for solids (PBEsol) [20] for the exchange correlation functional. The atomic PAW potentials were adopted from the PSlibrary.1.0 generated by A.Dal Corso [21]. The wave functions were expanded in plane-wave basis sets truncated at a cutoff energy of 50 Ry and the charge densities were truncated at 200 Ry. Brillouin zone integrations were performed on a 8× 8× 8 k-point grid, and the Marzari-Vanderbilt broadening [22] was applied with a smearing width of 5 mRy. The structural degrees of freedom were fully relaxed to obtain the optimized structural parameters.

The optimized structures from PAW calculation were used as the input for the MCA calculation. The MCA energy is defined as E_{mca}=E_{100}−E_{001}, where E_{001} and E_{100} are the total energies for the magnetization oriented along the [001] and [100] directions, respectively. Positive (negative) E_{mca} corresponds to easy c− axis (easy ab− plane) MCA.

The MCA energies were calculated using a full potential plane wave plus muffin-tin orbital (PMTO) approach, a fusion of the linear augmented plane waves (LAPW) and muffin-tin orbital (MTO) method [23–25]. The relativistic effects were treated by solving a scalar relativistic wave equation. Spin-orbit coupling (SOC) are included to attain the orbital moments and evaluate MCA. The method has been used to calculate the MCA energy in $Fe_{16}N_2$ [26]. Brillouin zone integrations were performed on a 24× 24× 24 k-point grid. The k-space integrations have been performed using the tetrahedron method [27,28]. Considering the strong correlation effect, the Gd 4f electrons were treated in a framework of DFT plus Hubbard U (DFT + U) [29–31]. In the DFT + U approach, the screened Coulomb and exchange energies of a chosen set of localized orbital (Gd 4f states) were added to the usual DFT functional and their orbital independent average was subtracted to avoid double counting. In the DFT + U calculations, we have used the Hubbard U = 6.7 eV and exchange parameter J = 0.7 eV for the Gd 4f electrons [32].

3. Results and discussion

3.1. Fe preferential site occupancy in $Gd(Co,Fe)_{12}B_6$

$GdCo_{12}B_6$ crystallizes with the trigonal $SrNi_{12}B_6$ structure (space group $R\bar{3}m$). In the primitive unit cell, there is one formula unit of $GdCo_{12}B_6$ with two inequivalent crystallographic sites for the Co atoms (18g and 18h). To evaluate the effects of Co substitution by Fe, one Fe atom was placed on each of the two Co sites in turn. As all single-Fe replacements on a given site (18g or 18h) are equivalent, only a single substitutional configuration needed to be checked for each cobalt site.

The structural parameters of $GdCo_{12-x}Fe_xB_6$ with x = 0 and 1 have been fully relaxed using the PAW method and are shown in Table 1. The experimental data are also listed in the table. As shown in the table, the lattice constants are underestimated by about 1%. The cohesion energy, E_c, for x = 0 is smaller than that for x = 1 by about 0.42 eV/f.u., indicating Fe doping reduces the structural stability of $GdCo_{12}B_6$. This is consistent with the fact that $GdCo_{12}B_6$ is a stable compound while $GdFe_{12}B_6$ does not exist. Indeed, $GdCo_{12-x}Fe_xB_6$ can only be prepared as far as x~3 [17].

Table 1
Calculated and experimental lattice constants, magnetic moments and cohesion energy (eV/f.u.) in $GdCo_{12-x}Fe_xB_6$ (x = 0,1).

	x = 0			x = 1		
	PAW	MTO	exp.	PAW	MTO	exp.
a (Å)	9.267	–	9.435	9.377	–	9.468
c (Å)	7.323	–	7.442	7.400	–	7.453
M_{Gd} (μ_B)	7.08	7.44	6.90	7.04	7.45	–
M_{Co}(18g) (μ_B)	− 0.34	− 0.24	− 0.41	− 0.27	− 0.23	–
M_{Co}(18h) (μ_B)	− 0.79	− 0.74	− 0.50	− 0.65	− 0.70	–
M_{Fe}(18h) (μ_B)	–	–	–	− 1.40	− 1.53	1.03
M_{tot} (μ_B/f.u.)	0.30	1.56	1.68	0.77	1.04	1.13
E_c (eV/f.u.)	− 128.58	–	–	− 128.16	–	–

The calculated cohesive energies E_c for Fe at the 18g and 18h sites are −128.00 eV/f.u and − 128.16 eV/f.u. in $GdCo_{11}Fe_1B_6$, respectively. The results indicate that Fe prefers to substitute for Co at the 18h site. The different substitution energies are the result of the different structural and chemical environments of the substituted sites. The Wigner-Seitz volumes (WSV) have been calculated for the two Co sites in $Gd(Co,Fe)_{12}B_6$ with DFT optimized structural parameters using a DIDO code [33]. The 18h site has a larger site volume (11.6 Å^3) than the 18g (11.2 Å^3) site. The metallic atomic radii are 1.26 Å and 1.25 Å for Fe and Co, respectively [34]. The replacement of Co by Fe will induce local strains due to the atomic size mismatch. To reduce the local strain, the larger Fe atoms favor the larger volume 18h site. This has been observed to be the dominant factor in Fe(Co) substitutions in a wide variety of rare-earth iron intermetallic compounds [35].

The substitution energy of Co by Fe can be defined as

$$E_{sub} = E_c(GdCo_{11}FeB_6) - E_c(GdCo_{12}B_6) \quad (1)$$

Based on the Maxwell-Boltzmann distribution [36], the occupation probability of Fe at each Co site in $Gd(Co,Fe)_{12}B_6$ can be expressed as

$$P_i = \frac{g_i \exp(-\Delta E_i/k_BT)}{\Sigma_i g_i \exp(-\Delta E_i/k_BT)} \quad (2)$$

Where g_i, ΔE_i, T and k_B are the multiplicity of the crystallographic site i, internal energy change (i.e. E_{sub}), temperature and Boltzmann's constant, respectively. The calculation details have been reported previously [37].

Fig. 1 displays the temperature dependence of the site occupancy of Fe in $GdCo_{12-x}Fe_xB_6$. As expected, Fe prefers the 18h site and the occupation bias decreases with increasing temperature. The results are in good agreement with the experimental results [16,17].

3.2. Electronic structure and magnetic moments in $Gd(Co,Fe)_{12}B_6$

The electronic structure of $GdCo_{12}B_6$ has been calculated using DFT + U. As shown in Fig. 2, the spin-projected total density of states (DOS) are mainly distributed between −8.5 eV and the Fermi

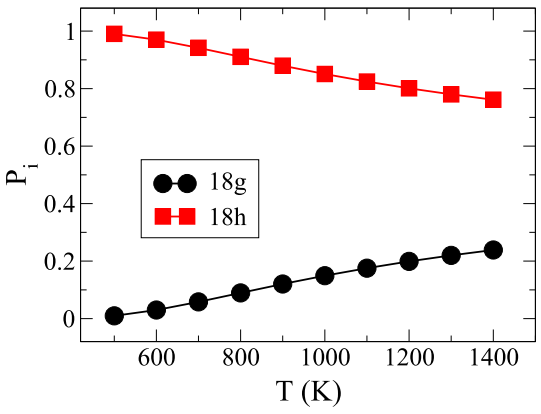

Fig. 1. Temperature dependence of the site occupation probability of Fe in $GdCo_{11}FeB_6$.

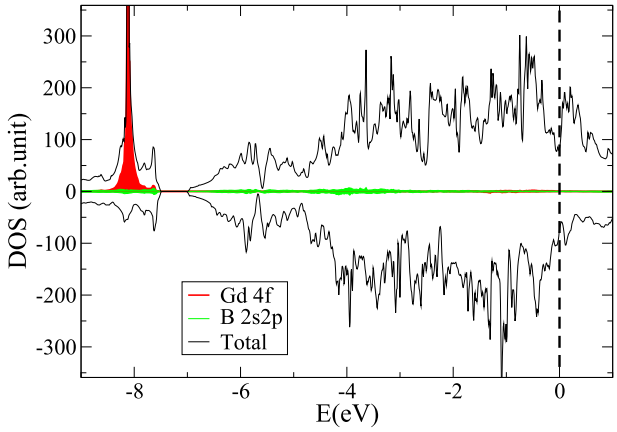

Fig. 2. Calculated spin-projected total DOS for in $GdCo_{12}B_6$. The red shaded areas show the DOS of Gd 4*f* contribution while the green shaded area is the DOS from boron atoms. (For interpretation of the references to colour in this figure legend, the reader is referred to the web version of this article.)

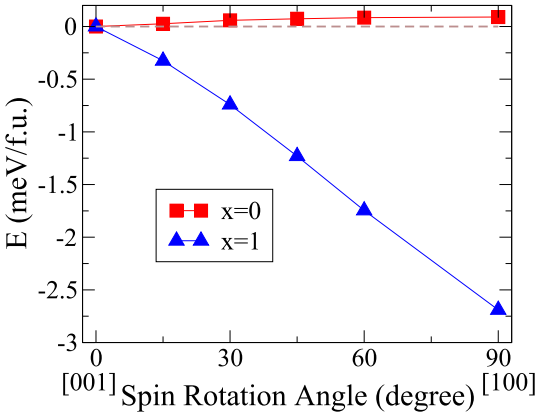

Fig. 3. Total energy relative to the ground state with magnetization along [001] direction as a function of spin quantization axis rotation in $GdCo_{12-x}Fe_xB_6$ with $x = 0$ and 1.

Level ($E_f = 0$). The green shaded areas show the electron states contributed by boron atoms. The red shaded areas show the Gd 4*f* contribution. As expected, the spin-majority (positive) 4*f* states of Gd are completely occupied and distributed around −8.1 eV. On the other hand the spin-minority (negative) 4*f* states of Gd are empty and well above the Fermi Level (not shown in Fig. 1). The DOS at E_f is dominated by *d*-like states, contributed mainly by the Co sublattices. Spin down DOS from the Co 3*d* electrons are the majority, resulting in a ferrimagnetic coupling between the Gd- and the Co-magnetic sublattices.

The magnetic moments have been derived from the DFT calculations (Table 1) for $GdCo_{12-x}Fe_xB_6$ with $x = 0$ and 1. As shown in Table 1, the calculated magnetic moments from PAW and PMTO are clearly different. In the PAW calculation, the Gd 4*f* electrons are treated as core states and the Gd atom gives a moment of 7.08 μ_B for $x = 0$. In the PMTO calculation, the Gd 4*f* electrons are treated as valence states with DFT + U method. The magnetic moment of Gd is 7.44 μ_B for $x = 0$. Similar results were observed for $x = 1$. As shown in Table 1, the total magnetization M_{tot} from the PMTO calculation is in much better agreement with the experimental results. The Co atoms at the 18*h* site (0.7 μ_B) have a larger magnetic moment than those at the 18*g* site (0.3 μ_B) due to the larger volume of the 18*h* site compared to that of the 18*g* site. It is interesting to note that the doped Fe atoms at their preferred 18*h* site carry a much larger magnetic moment (1.4–1.5 μ_B) than the Co atoms on the same site in $GdCo_{11}FeB_6$.

The moments determined here by DFT are in full agreement with those derived experimentally. Neutron diffraction and bulk magnetization give average cobalt moments of 0.46(2) μ_B and 0.44 μ_B respectively [17] with the Co(18*h*) moment being slightly larger than the Co(18*g*) moment. This compares well with the 0.5 μ_B average cobalt moment from DFT, although the difference between the two calculated moments is somewhat larger. For the iron moment, bulk magnetization suggests 1.2(1) μ_B/Fe, while neutron diffraction give a much less certain estimate of 2.5± 1.0 μ_B/Fe [17]. Both experimental estimates are consistent with the 1.4–1.5 μ_B calculated here.

3.3. Magneto-crystalline anisotropy energy in $Gd(Co,Fe)_{12}B_6$

The MCA energy E_{mca} has been calculated in $Gd(Co,Fe)_{12}B_6$ by the PMTO method. Fig. 3 shows the MCA energy as a function of spin quantization axis rotation in $GdCo_{12-x}Fe_xB_6$ with x=0 and x=1.

It is clear that undoped $GdCo_{12}B_6$ shows a very weak easy *c*− axis MCA, and this is consistent with the suggestion from the neutron diffraction study that while the order is essentially axial in nature, the moments are canted by at least 15° from the *c*− axis at 4 K in $GdCo_{12}B_6$ [17]. By contrast, $GdCo_{11}FeB_6$ clearly has a moderate easy *ab*− plane MCA. The MCA energies E_{mca} for x = 0 and x = 1 are 90 μeV/f.u. and − 2690 μeV/f.u., respectively. This factor of 30 change in MCA associated with replacing a one (of twelve) cobalt atoms by an iron atom (a doping level of ~ 8%) is consistent with the observation that even a doping level of 0.5% is sufficient to lead to planar ordering [9,38].

Iron doping will distort the crystal structure in addition to causing changes in the electronic and magnetic behavior in $Gd(Co,Fe)_{12}B_6$. To understand the change of MCA induced by doping with Fe, the MCA energy has been calculated as a function of the relative lattice constant ratio δ in $GdCo_{12}B_6$, where $\delta=(c/a)/(c_0/a_0)$ and a and c are the lattice constants while a_0 and c_0 are the optimized lattice constants of $GdCo_{12}B_6$. As shown in Fig. 4, the lattice distortion has very little effect on the MCA in $GdCo_{12}B_6$. These results imply that the change of MCA comes mainly from electronic and magnetic factors.

The microscopic origin of MCA is from spin-orbital coupling (SOC). The SOC of 3*d* electrons can be considered as perturbation. The first order perturbation terms are zero due to the angular moment quenching in the solid. The SOC energy can be expressed,

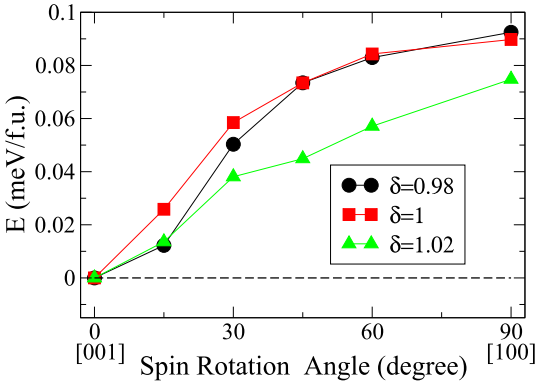

Fig. 4. Total energy relative to the ground state with magnetization along [001] direction as a function of spin quantization axis rotation in $GdCo_{12}B_6$ with relative lattice ratio δ = 0.98, 1 and 1.02. Where $\delta=(c/a)/(c_0/a_0)$ a and c are lattice constants while a_0 and c_0 are optimized lattice constants.

based on second order perturbation theory [39–41], as

$$E_{SOC} = \xi^2 \sum_{n_o,k_u} \frac{\left|\langle n|L\cdot S|k\rangle\right|^2}{E_n - E_k} \quad (3)$$

where $|n\rangle$ and $|k\rangle$ denote eigenvectors of the unperturbed Hamiltonian and E_n and E_k are the associated energy eigenvalues. For the case with both $|n\rangle$ and $|k\rangle$ states are occupied or unoccupied, there is a cancellation of these terms in the sum. The remained terms are those coupled occupied ($|n\rangle_o$) and unoccupied ($|k\rangle_u$) states. Since the SOC is inversely proportional to the energy difference between unoccupied and occupied states, the most important contributions are from the states just below and above the Fermi level.

The orbital magnetic moment ($M_{orb.}$) is related to SOC and MCA. In case the spin-flip contribution can be neglected, MCA is proportional to the orbital moments [42]. However, the simple corresponding relation will be invalid when spin-flip is important [41,43]. It is interesting that the site/atom resolved $M_{orb.}$ show almost linear variation as the spin quantization axis rotates from [001] to [100] direction in $GdCo_{12-x}Fe_xB_6$ with x=0 and x=1 (Fig. 5). For x=0, $M_{orb.}$ for the Gd site becomes slightly more negative while that of Co sites (18*g* and 18*h*) become more positive by approximately the same amount as the spin axis rotates from [001] to [100]. On the other hand, for x=1, while $M_{orb.}$ for Gd and the Co 18*g* sites show moderate negative tendency on rotating from [001] to [100], $M_{orb.}$ for Fe(18*h*) exhibits a very rapid change. The doped Fe greatly changes the dependence of the orbital moment of the Co(Fe) sublattice on the spin rotation angle in the compound with x=1. The Fe orbital moment seems almost quenched along [001] direction for x=1. Here, a supercell approximation is employed to mimic alloying behavior so the more physical parameter is the average $M_{orb.}$ at the 18*h* site. The average $M_{orb.}$ at the 18*h* site for x=1 is almost triple as that for x=0, and changes by about 20–30% as the spin quantization axis changes from [001] to [100] direction.

As show in Fig. 5, the absolute value of $M_{orb.}$ for Gd and Co increases and decreases almost linearly, respectively, for x=0 as the spin quantization axis rotates from [001] to [100]. However, all the $M_{orb.}$ absolute value for Gd, Co and Fe increases almost linearly for x=1 upon rotating spin axis from [001] to [100]. The spin axis dependence of $M_{orb.}$ for x=0 is clearly opposite to that for x=1, indicating a Fe-doping induced change of the orbital moment anisotropy. Fe-doping causes abrupt changes of both the anisotropy of orbital moment and the magneto-crystalline anisotropy (MCA). Although there is no quantitative relationship between $\delta M_{orb.}$ and E_{mca} due to the spin-flip contribution to E_{SOC}, we believe that both of them are related to changes in the electronic structure near Fermi level upon Fe-doping. One possible explanation is that the electron band filling near the Fermi level is changed upon partially replacing Co ($3d^7$) by Fe ($3d^6$) with fewer 3*d* electrons. This is responsible for the changes of the $M_{orb.}$ anisotropy and MCA in the compound with x=1. The sensitive behavior of MCA to band filling has been reported in $Li_2(Li_{1-x}T_x)N$ with T = Mn, Fe, Co and Ni by Ke and van Schilfgaarde [41].

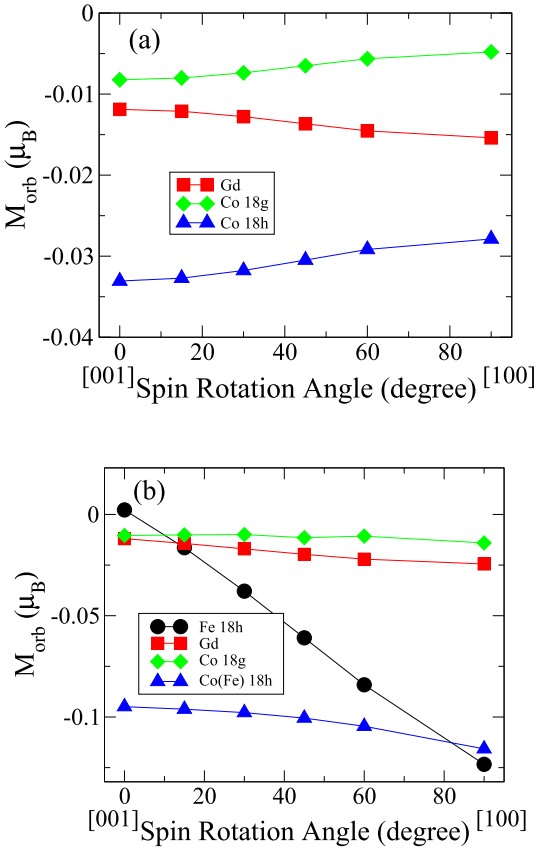

Fig. 5. Atomic orbital magnetic moment as a function of spin quantization axis rotation in $GdCo_{12-x}Fe_xB_6$ with x = 0 (a) and 1 (b).

4. Summary

$GdCo_{12-x}Fe_xB_6$ has been investigated by DFT + U. The total energy calculations show that the Fe atoms prefer to substitute for Co at the 18*h* rather than the 18*g* site, with an energy gain of 0.16 eV/f.u. Gd has a magnetic moment of 7.3 μ_B that is ordered antiparallel to the Co(Fe) sublattice. The Co atoms in $GdCo_{12}B_6$ carry magnetic moments of − 0.3 μ_B and − 0.7 μ_B at the 18*g* and 18*h* sites respectively. The doped Fe atoms at the 18*h* site have a magnetic moment of 1.5 μ_B. The MCA energy calculations indicate that $GdCo_{12}B_6$ has a weak easy *c*− axis MCA with E_{mca} = 90 μeV/f.u. However, $GdCo_{11}FeB_6$ displays an easy *ab*− plane MCA with E_{mca} = −2690 μeV/f.u. The spin reorientation induced by doping Fe is related the electronic structure change near Fermi Level and the different contributions of Co and Fe to the MCA in $GdCo_{12-x}Fe_xB_6$. As the ordering directions for the other $RCo_{12}B_6$ compounds have all been derived from ^{57}Fe-doped samples, a re-evaluation of these compounds may be necessary due to the strong effect of Fe on the MCA in this system.

Acknowledgments

Financial support for this work was provided by the Natural Sciences and Engineering Research Council of Canada and the Fonds Québécois de la Recherche sur la Nature et les Technologies.

References

[1] J.J. Croat, J.F. Herbst, R.W. Lee, F.E. Pinkerton, J. Appl. Phys. 55 (1984) 2078.
[2] M. Sagawa, S. Fujimura, M. Togawa, H. Yamamoto, Y. Matsuura, J. Appl. Phys. 55 (1984) 2083.
[3] J.F. Herbst, Rev. Mod. Phys. 63 (1991) 819 (and the references therein).
[4] K. Niihara, S. Yajima, Chem. Lett. 1 (1972) 875.
[5] K.H.J. Buschow, D.B.D. Mooij, H.M. van Noort, J. Less-Common Met. 125 (1986) 135.
[6] M. Rosenberg, M. Mittag, K.H.J. Buschow, J. Appl.Phys. 63 (1988) 3586–3588.
[7] M. Mittag, M. Rosenberg, K.H.J. Buschow, J. Magn. Magn. Mater 82 (1989) 109–117.
[8] G.F. Zhou, X. Li, F. R de Boer, K.H.J. Buschow, Phys. B 177 (1992) 286–290.
[9] M. Rosenberg, T. Sinnemann, M. Mittag, K.H.J. Buschow, J. Alloys Compd. 182 (1992) 145–156.
[10] J.M. Cadogan, S.J. Campbell, X.L. Zhao, E. Wu, Aust. J.Phys. 46 (1993) 679.
[11] Z. Arnold, O. Isnard, H. Mayot, M. Misek, J. Kamarad, J. Magn. Magn. Mater 322

(2010) 1117–1119.
[12] G.I. Miletic, Z. Blazina, J. Magn. Magn. Mater 323 (2011) 2340–2347.
[13] O. Isnard, Y. Skourski, L.V.B. Diop, Z. Arnold, et al., J. Appl. Phys. 111 (2012) 093916.
[14] E. Wu, J.M. Cadogan, S.J. Campbell, X.L. Zhao, Hyperfine Interact. 94 (1994) 1903–1908.
[15] X. Zhao, J.M. Cadogan, S.J. Campbell, J. Magn. Magn. Mater 140–144 (1995) 959–960.
[16] N.R. Lee-Hone, D.H. Ryan, O. Isnard, L.V.B. Diop, J.M. Cadogan, J. Appl. Phys. 113 (2013) 17E119.
[17] L.V.B. Diop, O. Isnard, N.R. Lee-Hone, D.H. Ryan, J.M. Cadogan, J. Phys. Condens. Matter 25 (2013) 316001.
[18] P. Giannozzi, S. Baroni, N. Bonini, M. Calandra, et al., J. Phys. Condens. Matter 21 (2009) 395502.
[19] P.E. Blöchl, Phys. Rev. B 50 (1994) 17953.
[20] a J.P. Perdew, K. Burke, M. Ernzerhof, Phys. Rev. Lett. 77 (1996) 3865;
b J.P. Perdew, et al., Phys. Rev. Lett. 100 (2008) 136406.
[21] A. Dal Corso, Comput. Mater. Sci. 95 (2014) 337–350.
[22] Nicola Marzari, David Vanderbilt, Alessandro De Vita, M.C. Payne, Phys. Rev. Lett. 82 (1999) 3296.
[23] O.K. Andersen, Phys. Rev. B 12 (1975) 3060.
[24] M. Methfessel, M. van Schilfgaarde, R.A. Casali, in: H. Dreysse (Ed.), Electronic Structure and Physical Properties of Solids: the Use of LMTO Method, Springer-Verlag, Berlin, 2000, p. 114.
[25] T. Kotani, M. van Schilfgaarde, Phys. Rev. B 81 (2010) 125117.
[26] L. Ke, K.D. Belashchenko, M. van Schilfgaarde, T. Kotani, V.P. Antropov, Phys. Rev. B 88 (2013) 024404.
[27] O. Jepsen, O.K. Andersen, Solid State Commun. 9 (1971) 1763.
[28] P. Blochl, O. Jepsen, O.K. Andersen, Phys. Rev. B 49 (1994) 16223.
[29] V.I. Anisimov, J. Zaanen, O.K. Andersen, Phys. Rev. B 44 (1991) 943.
[30] A.I. Lichtenstein, V.I. Anisimov, J. Zaanen, Phys. Rev. B 52 (1995) R5467.
[31] M. Richter, J. Phys. D. Appl. Phys. 31 (1998) 1017.
[32] D. van der Marel, G.A. Sawatzky, Phys. Rev. B 37 (1988) 10674.
[33] E. Koch, W. Fischer, Z. Kristallogr 211 (1996) 251.
[34] [Online]. Available: www.kayelaby.npl.co.uk, Kaye and Laby Tables of Physical and Chemical Constants (Online Edition).
[35] L.X. Liao, Z. Altounian, D.H. Ryan, Phys. Rev. B 47 (1993) 11230–11241.
[36] R.C. Tolman, The Principles of Statistical Mechanics, Dover Pub. Inc., New York, 1979.
[37] X.B. Liu, J.P. Liu, Qiming Zhang, Z. Altounian, Comput. Mater. Sci. 85 (2014) 186.
[38] X. Zhao (1996) PhD Thesis UNSW, Australia.
[39] V. Antropov, L. Ke, D. Aberg, Solid State Commun. 194 (2014) 35.
[40] E.K. Delczeg-Czirjak, A. Edstrom, M. Werwinski, J. Rusz, N.V. Skorodumova, L. Vitos, O. Eriksson, Phys. Rev. B 89 (2014) 144403.
[41] L. Ke, M. van Schilfgaarde, Phys. Rev. B 92 (2015) 014423.
[42] P. Bruno, Phys. Rev. B 39 (1989) 865–868.
[43] C. Andersson, B. Sanyal, O. Eriksson, L. Nordstrm, O. Karis, D. Arvanitis, T. Konishi, E. Holub-Krappe, J. Dunn, Phys. Rev. Lett. 99 (2007) 177207.